Max-Planck-Institut
für Meteorologie

REPORT No. 103

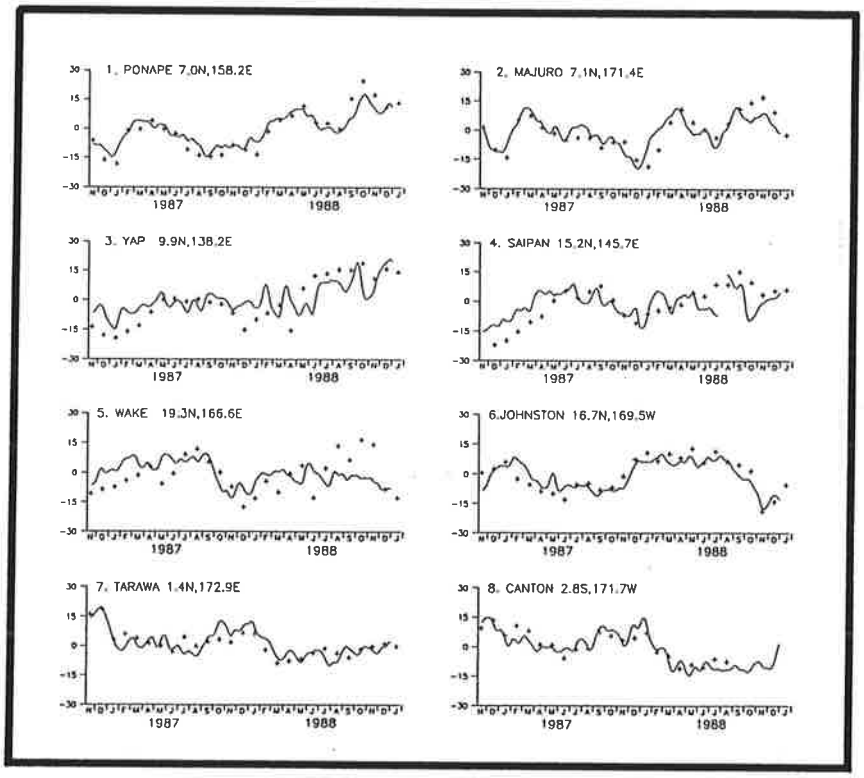

MODES OF OCEAN VARIABILITY IN THE TROPICAL PACIFIC AS DERIVED FROM GEOSAT ALTIMETRY

by

JIANSHENG ZOU • MOJIB LATIF

HAMBURG, APRIL 1993

AUTHORS:

Jiansheng Zou

Institut für Meereskunde
Universität Hamburg
Troplowitzstraße 7
D–2000 Hamburg 54
F.R.G.

Mojib Latif

Max–Planck–Institut
für Meteorologie

MAX–PLANCK–INSTITUT
FÜR METEOROLOGIE
BUNDESSTRASSE 55
D–2000 HAMBURG 13
F.R. GERMANY

Tel.: +49 (40) 4 11 73–0
Telex: 211092 mpime d
Telemail: MPI.METEOROLOGY
Telefax: +49 (40) 4 11 73–298

REPb103

Modes of Ocean Variability in the Tropical Pacific as Derived from Geosat Altimetry

Jiansheng Zou
Institut für Meereskunde, Universität Hamburg
Troplowitzstr. 7, D-2000 Hamburg 54, Germany

and

Mojib Latif
Max-Planck-Institut für Meteorologie
Bundesstr. 55, D-2000 Hamburg 13, Germany

Abstract

Satellite-derived (GEOSAT) sea surface height anomalies for the period November 1986 to August 1989 were investigated in order to extract the dominant modes of climate variability in the tropical Pacific. Four modes are identified by applying the POP technique. The first mode has a time scale of about 3 months and can be identified with the first baroclinic equatorial Kelvin wave mode. The second mode has a time scale of about six months and describes the semi-annual cycle in tropical Pacific sea level. Equatorial wave propagation is also crucial for this mode. The third mode is the annual cycle which is dominated by Ekman dynamics. Wave propagation or reflection are found to be unimportant. The fourth mode is associated with the El Niño/Southern Oscillation (ENSO) phenomenon. The ENSO mode is found to be consistent with the 'delayed action oscillator' scenario.

The results are substantiated by a companion analysis of the sea surface height variability simulated with an oceanic general circulation model (OGCM) forced by observed wind stresses for the period 1961 to 1989. The modal decomposition of the sea level variability is found to be similar to that derived from the GEOSAT data. The high consistency between the satellite and the model data indicates the high potential value of satellite altimetry for climate modeling and forecasting.

Corresponding author address: Dr. M. Latif, Max-Planck-Institut für Meteorologie, Bundesstr. 55, D-2000 Hamburg-13, Germany

ISSN 0937–1060

1. Introduction

The verification and further development of ocean general circulation models depends critically on the availability of adequate forcing and verification data. Also the application of coupled ocean-atmosphere models to short-range climate predictions requires a good data base for properly specifying the initial state of the coupled system. At present, however, there is a significant lack in data, especially over the oceans. Therefore, satellite-derived are data becoming more and more important in climate research because the quality of satellite data has significantly increased during the last few years, and the use of satellites is on the long term, the only means of obtaining climate data in near real time in adequate temporal and spatial resolution. The only satellite-derived oceanic quantity hitherto used to analyze the oceanic state is sea surface temperature (SST) (Reynolds (1988)), but recent studies indicate that other important parameters, such as sea level and surface wind stress, can be measured with some accuracy from space. Moreover, Picaut et al. (1990) showed that it is also possible to derive low-frequency variations in equatorial Pacific zonal currents from satellite-derived sea level.

Sea level is particularly interesting because it is an integrated quantity and therefore contains also some information from subsurface levels. Many studies using data from the GEOSAT mission have focussed on the tropical Pacific (e. g. Tai (1988), Tai et al. (1989), Cheney et al. (1989), Cheney and Miller (1990), White and Tai (1990), White et al. (1990)), and the high value of such data in understanding climate variability in this region has been demonstrated. Other studies related to the GEOSAT mission can be found in a special volume of the Journal of Geophysical Research (1990).

The GEOSAT data set, the longest available satellite-derived sea level data set, is re-analyzed in this paper using the POP-technique (Hasselmann (1988), Storch et al. (1988)). The POP-technique estimates not only the dominant variability patterns but also their corresponding time scales. The use of such a sophisticated statistical method to analyze the sea level variability is necessary because the different modes in the tropical Pacific do not have well

separated time scales. Thus, one cannot distinguish them clearly by considering case studies or applying Complex Empirical Orthogonal Functions (CEOFs) which average in frequency domain.

The results of the POP-analysis are compared to those from a similar analysis of the output of an oceanic general circulation model (OGCM). Ocean models have been shown to simulate realistically sea level variability in the tropical Pacific (e. g. Busalacchi et al. (1983), Latif (1987)). By verifying against model data, one can estimate not only the reliability of the GEOSAT data but also to what extent the satellite data are consistent with the ocean model data, and whether they can be used successfully in assimilation experiments.

Despite the short time period covered by the GEOSAT data set (Nov. 1986 - Aug. 1989), the set provides a clear description of the different variability modes in the tropical Pacific. Our analysis indicates the existence of at least four modes, a Kelvin wave mode, the semi-annual cycle, the annual cycle, and an interannual mode with a time scale of about three years, the El Niño/Southern Oscillation (ENSO) mode.

This paper is organized as follows: In section two the data and the POP-technique are described. The satellite-derived sea levels are compared with tide gauge data in section three. Section four deals with the results of the POP-analysis. The paper is concluded in section five.

2. Data and statistical analysis technique

2.1 Satellite wind data

The GEOSAT data used in this study are the so-called T2 - Geophysical Data Records (T2-GDRs) which cover the time period November 1986 to September 1989. Relative to the original GDRs, the T2-GDRs, described by Cheney et al. (1991) and Miller and Cheney (1990), were produced using an improved representation of the satellite orbit and applying more realistic water vapour corrections based on satellite measurements (SSM/I and TOVS). The altimeter data profiles were taken over the area 50°S to 40°N and 80°E to 50°W, which is considerably larger than the region of interest, and even includes part of the Indian

Ocean. The choice of this relatively large domain is important to avoid a damping of oceanic signals with long wavelengths. We used linear functions to fit the satellite radial orbital error. The altimeter along-track sea level deviations were generated using the conventional collinear analysis method (Cheney et al. (1989)).

The objective analysis method (Bretherton et al. (1976)) was applied to interpolate the altimeter along-track data to selected locations. Data were constructed for the tropical Pacific and cover the region 20°N - 20°S, 120°E - 90°W, with a resolution of 2° (latitude) x 10° (longitude). Sea level anomalies were computed relative to the January 1987 - December 1988 mean. The time resolution is 5 days. In order to derive the characteristic low-level wind patterns which force the sea level variations, associated regression patterns were computed for the 850 hPa level. Instantaneous 850 hPa winds were obtained from the analysis of the European Centre for Medium-Range Forecasts (ECMWF).

2.2 Verification data

As verification data we use tide gauge data (Wyrtki et al. (1988)). These data were used by Latif and Flügel (1991) in a statistical investigation of the low-frequency variability in the tropical Pacific. We also use sea levels simulated by an oceanic general circulation model (OGCM). The model, described in detail by Latif (1987) and Barnett et al. (1991), carries sea level as a prognostic variable and simulates realistically the observed sea level variations in the tropical Pacific. The OGCM was forced by observed monthly wind stresses for the period 1961 to 1989 taken from the Florida State University (FSU) data set (Goldenberg and O'Brien (1981), Legler and O'Brien (1984)). We used the whole 29-year data set in the statistical analysis, in order to increase the statistical significance of our results, especially with respect to the low-frequency variability.

Additionally, two sensitivity runs of 50 years duration were performed. In the first sensitivity run the OGCM was forced by random wind stress anomalies added to the mean January wind stresses, in order to derive the normal modes of the tropical Pacific. The random wind stress anomaly fields were constructed from the first ten Empirical Orthogonal Functions (EOFs) of the observed stresses. The corresponding EOF time series are white, and the variance explained by each EOF was taken from the observations. In the second

sensitivity run the OGCM was forced by the seasonal cycle of the wind stress only.

The annual mean sea level was subtracted from all data sets prior to the POP analyses, and time filtering was applied. Two POP analyses were performed. First, in order to derive variability modes with time scales less than the annual cycle, the GEOSAT data were band-pass filtered retaining variability with periods of one to ten months, and the POP analysis was restricted to the first two years and the region 10°N to 10°S only. Second, a low-pass filter retaining variability with time scales longer than 3 months was applied to derive the annual cycle and low-frequency modes from the GEOSAT data, and the POP analysis was applied to the complete time period and the region 20°N to 20°S.

2.3 POP-analysis

Our statistical investigation of the modes of climate variability in the tropical Pacific is based on the method of 'Principal Oscillation Patterns' (POPs) which is designed to extract the dominant modes of variability from a multi-dimensional data set (Hasselmann (1988), Storch et al. (1988)). The POPs are the eigenvectors of the system matrix obtained by fitting the data to a multivariate first order Markov process. POPs are in general complex with real part p_1 and imaginary part p_2. The corresponding complex coefficient time series satisfy the standard damped harmonic oscillator equation, so that the evolution of the system in the two-dimensional POP space can be interpreted as a cyclic sequence of spatial patterns:

$$\ldots\ldots \rightarrow p_1 \rightarrow -p_2 \rightarrow -p_1 \rightarrow p_2 \rightarrow p_1 \rightarrow \ldots\ldots \qquad (1)$$

The characteristic period to complete a full cycle will be referred to as 'rotation period' and the e-folding time for exponential decay as 'damping time'. Both time scales are estimated as part of the POP-analysis. As described by Hasselmann (1988), the POP-technique as opposed to complex EOFs has the advantage of providing information about the frequency structure of the cross-spectrum by identifying the spectral peaks (inverse rotation

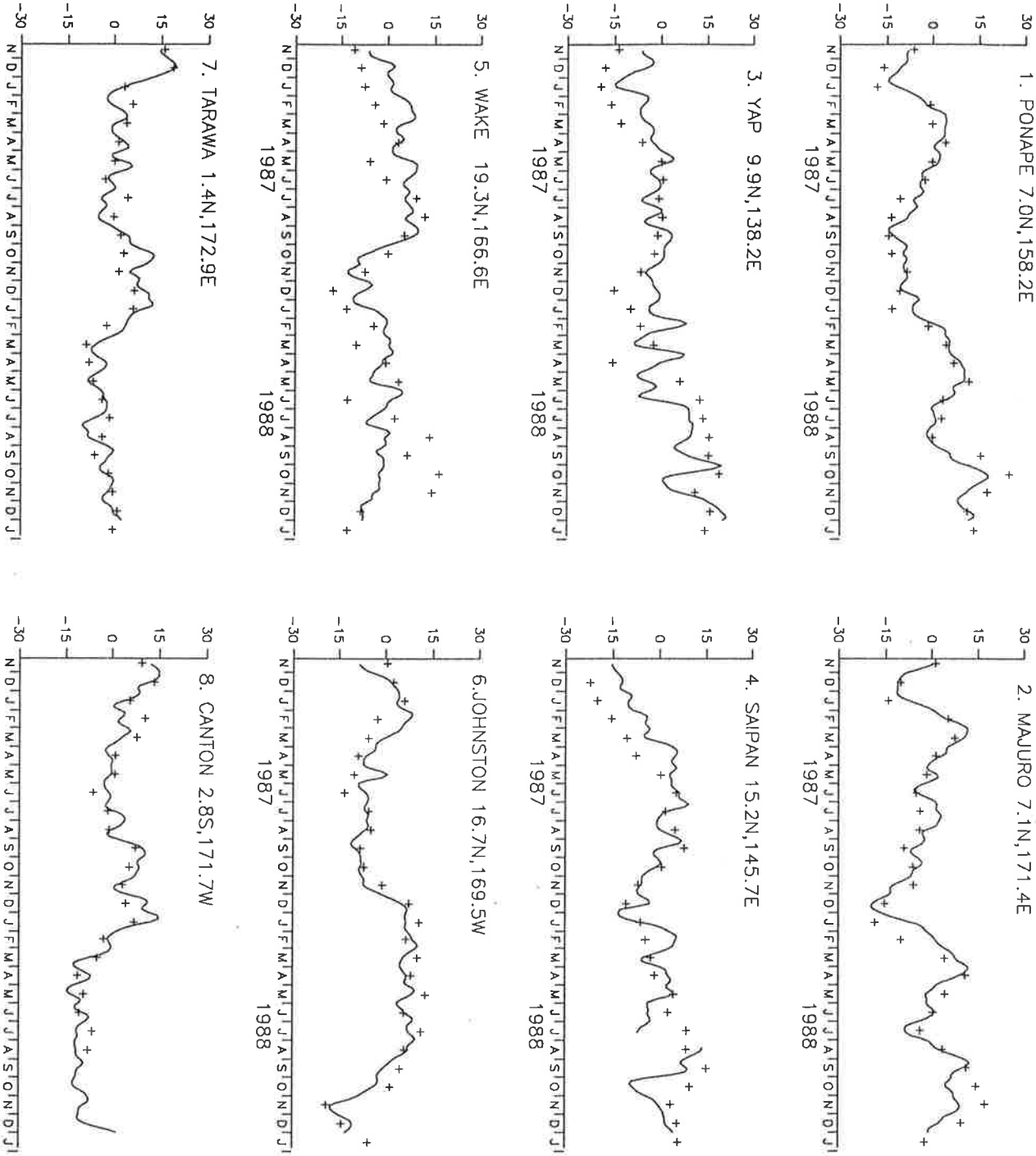

Figure 1: Comparison of satellite-derived and island station sea levels for selected locations for the period November 1986 to January 1989. The corresponding statistics are given in Table 1.

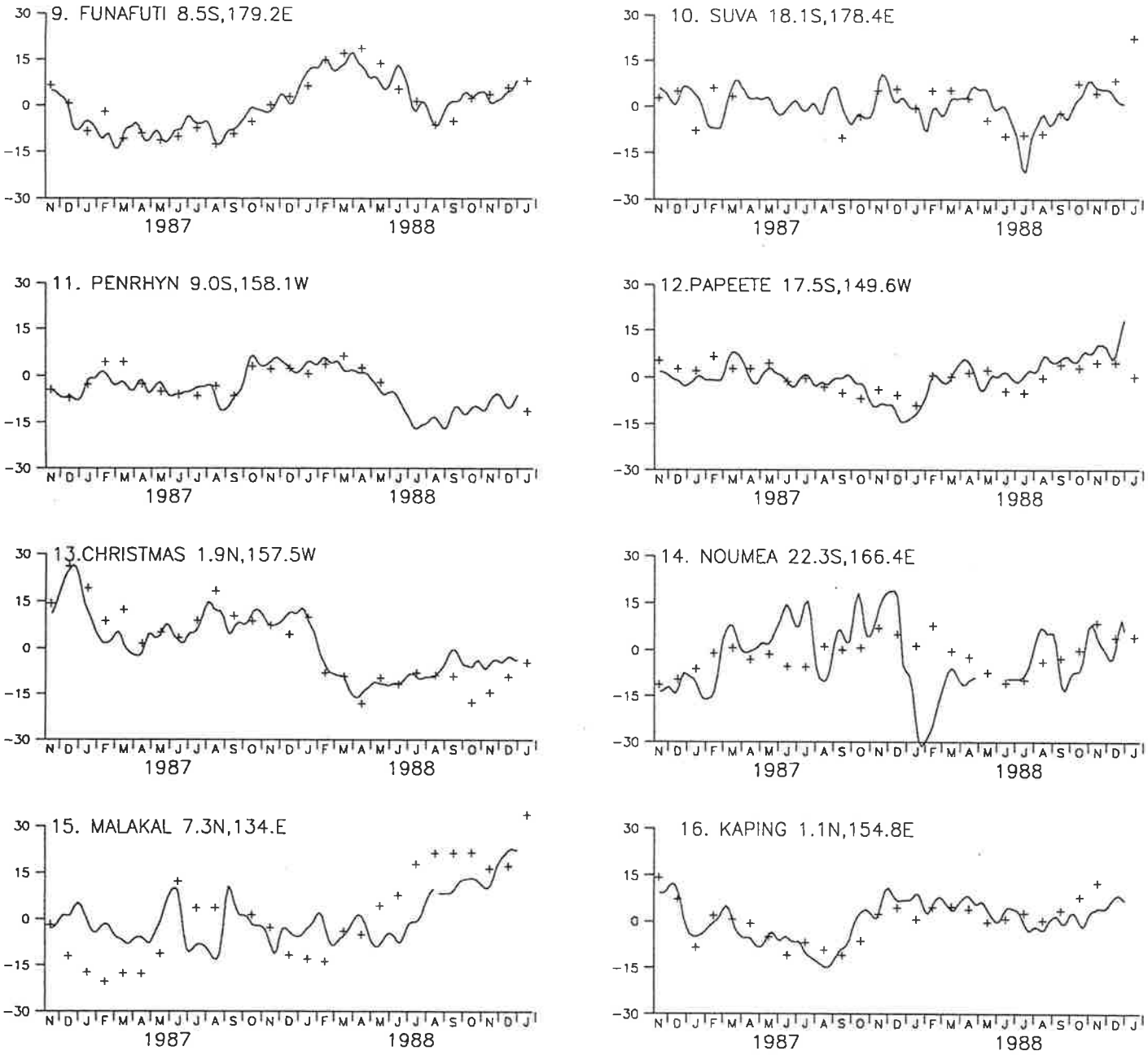
9. FUNAFUTI 8.5S,179.2E
10. SUVA 18.1S,178.4E
11. PENRHYN 9.0S,158.1W
12.PAPEETE 17.5S,149.6W
13.CHRISTMAS 1.9N,157.5W
14. NOUMEA 22.3S,166.4E
15. MALAKAL 7.3N,134.E
16. KAPING 1.1N,154.8E
30
15
0
-15
-30
N D J F M A M J J A S O N D J F M A M J J A S O N D J
1987
1988

Fig. 1, cont.

periods) and peak widths (inverse damping times) associated with different patterns. In order to investigate the spatial characteristics of the low-level wind fields which force the sea level variability, associated regression patterns were calculated by simply regressing the components of the wind field on the POP coefficient time series.

3. Comparison with tide gauge data

Tide gauge sea levels are the only observational data available for verifying the satellite-derived sea levels. The altimetric sea levels were interpolated objectively onto the tide gauge locations, in order to compare the two data sets. Overall, the altimetric sea levels are highly correlated with the tide gauge data, as can be inferred from Fig. 1 which shows time series of the observed and altimetric sea levels at selected locations. Correlation coefficients are of the order of 0.8, whereas the RMS-error does not exceed a few centimeters. Thus, the GEOSAT T2-GDRs are improved significantly relative to the original GDRs (e. g. Tai et al. (1989)). Table 1 shows a comparison of the verification results obtained using the original and T2- GDRs. Poleward of 20° in both hemispheres, the results are still unsatisfying. Our main focus in this paper, however, is the equatorial region. We therefore restrict ourselves here to the region 20°N to 20°S, where the altimetric sea levels are in excellent agreement with the tide gauge data.

4. Variability modes

The spatial resolution of the tide gauge data is not good enough to decompose the sea level variability into different variability modes. Instead, we used the OGCM sea levels to verify the variability modes derived from the GEOSAT data set. The model sea levels have been shown to be highly consistent with the tide gauge observations (Latif et al. (1987)). However, we show results from the POP analyses of the GEOSAT sea levels only, because the results of the analyses of the ocean model data yielded very similar results. Major differences between the GEOSAT and model data are indicated in the text below. We summarize the results of the POP analyses of the GEOSAT and OGCM sea levels

Table 1

	Islands	Positions	σt(cm)	Previous results R	δ(cm)	σs/σt	New results R	δ(cm)	σs/σt
1.	Ponape	7.0°N,158.2°E	11.1	0.92	6.9	0.44	0.96	4.2	0.77
2.	Majuro	7.1°N,171.4°E	9.1	0.72	6.3	0.69	0.84	5.0	0.85
3.	Yap	9.9°N,138.2°E	11.6	0.42	10.6	0.40	0.61	9.3	0.67
4.	Saipan	15.2°N,145.7°E	9.3	0.36	8.7	0.29	0.53	8.1	0.71
5.	Wake	19.3°N,166.6°E	9.1	0.30	8.7	0.37	0.25	9.4	0.63
6.	Johnston	16.7°N,169.5°W	8.6	0.81	5.1	0.80	0.81	5.0	0.83
7.	Tarawa	1.4°N,172.9°E	6.4	0.78	4.1	0.89	0.81	4.2	1.11
8.	Canton	2.8°S,171.7°W	7.2	0.78	4.5	0.72	0.89	4.0	1.21
9.	Funafuti	8.5°S,179.2°E	9.0	0.88	4.5	0.73	0.90	3.9	0.9
10.	Suva	18.1°S,178.4°E	6.2	0.21	6.8	0.68	0.23	7.5	0.94
11.	Penrhyn	9.0°S,158.1°W	4.3	0.74	3.2	1.07	0.8	2.7	0.98
12.	Papeete	17.5°S,149.6°W	4.1	0.43	5.2	1.34	0.65	3.9	1.22
13.	Christmas	1.9°N,157.5°W	12.2	0.65	9.3	0.62	0.91	5.3	0.78
14.	Noumea	22.3°S,166.4°E	3.5	---	---	---	---	---	---
15.	Malakal	7.3°N,134.5°E	13.6	0.22	13.3	2.37	0.51	11.5	0.60
16.	Kapingamarangi	1.1°N,154.8°E	6.6	-0.13	8.2	0.61	0.77	4.5	0.97
17.	Nauru	0.5°S,166.9°E	7.2	0.60	5.7	0.69	0.72	5.1	0.90
18.	French	23.9°S,166.3°W	11.6	0.39	11.0	0.16	-0.01	12.9	0.46
19.	Honolulu	21.3°N,157.9°W	5.7	0.28	6.4	0.84	0.56	5.7	1.12
20.	Rarotonga	21.2°S,160.0°W	7.5	0.65	5.8	0.53	0.43	7.0	0.68
21.	Fanning	3.9°N,159.4°W	9.3	0.90	4.3	0.73	0.89	4.3	0.85
22.	Rikitea	23.1°S,134.6°W	4.5	0.10	4.8	0.53	0.41	4.6	0.89
23.	Easter	27.2°S,109.5°E	4.4	0.03	4.8	0.45	-0.09	6.4	0.98
24.	Honiara	9.4°S,160.0°E	---	---	---	---	---	---	---
25.	Rabaul	4.2°S,152.1°E	---	---	---	---	---	---	---
26.	Nuku hiua	8.9°S,140.1°W	5.6	0.21	5.5	0.61	0.72	3.6	0.75
27.	Chichijima	27.1°N,142.2°E	8.1	-0.14	9.1	0.43	0.03	11.2	0.99
28.	Midway	28.2°N,177.4°W	6.5	0.29	6.3	0.55	0.14	6.9	0.57
29.	Truk	7.5°N,151.9°E	6.6	0.65	4.6	0.5	0.76	4.3	0.95
30.	Kwajalein	8.7°N,167.7°E	6.6	0.91	3.1	1.15	0.85	4.6	1.30
31.	Santa Cruz	0.9°S,90.3°W	10.3	0.60	6.7	0.28	---	---	---
32.	Balta	0.43°S,90.3°W	10.3	0.73	4.7	0.30	---	---	---

Comparison of the GEOSAT sea levels with the tide gauge data (new results). The results of the original GEOSAT GDRs are also given (previous results). Given are the correlatios (R), the RMS error (δ) and the ratio of the standard deviations (σs/σt).

Table 2

Mode	Origin of data	Rotation period [mo]	Damping time [mo]
Kelvin wave	GEOSAT	3	3
Kelvin wave	OGCM	not resolved	
semi-annual cycle	GEOSAT	6	11
semi-annual cycle	OGCM	7	4
annual cycle	GEOSAT	12	20
annual cycle	OGCM	12	18
ENSO	GEOSAT	38	34
ENSO	OGCM	33	32

Table of variability modes as derived from the GEOSAT and the ocean model data. The rotation periods and the damping times are given in months.

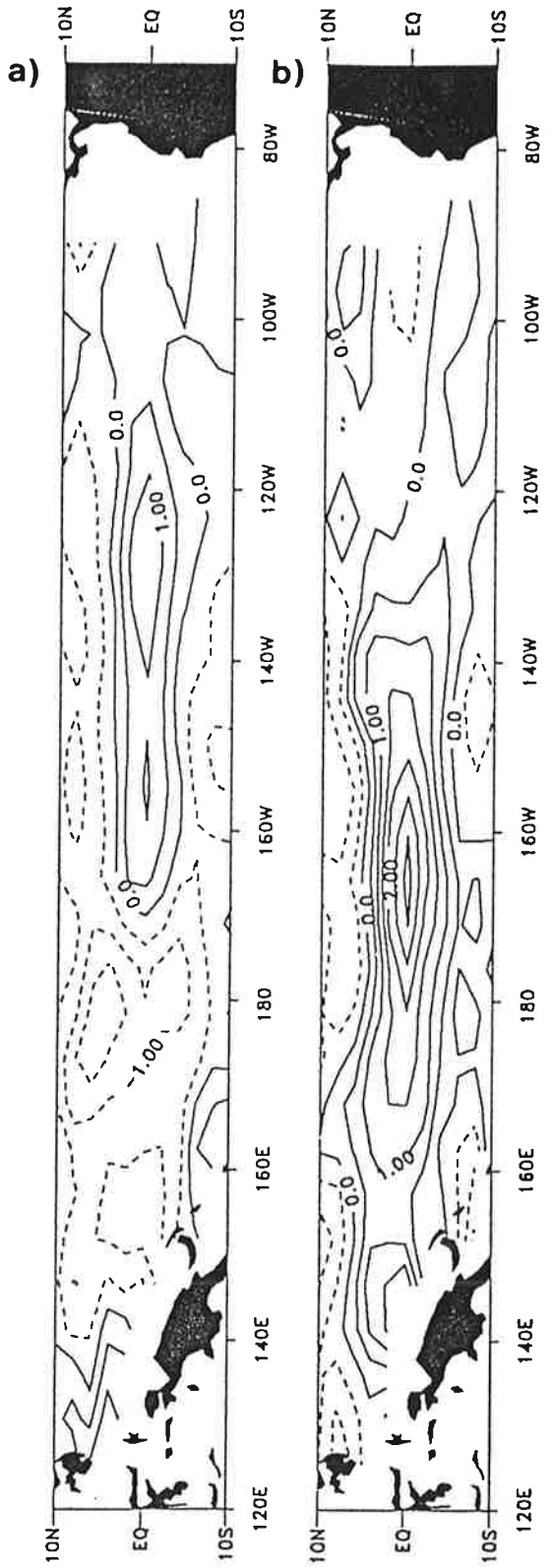

CONTOUR FROM -4.0000 TO 4.0000 CONTOUR INTERVAL OF 0.50000 PT(3,3)= 0.90000+100

Figure 2: Spatial patterns of the Kelvin wave POP mode. a) Real part, b) imaginary part.

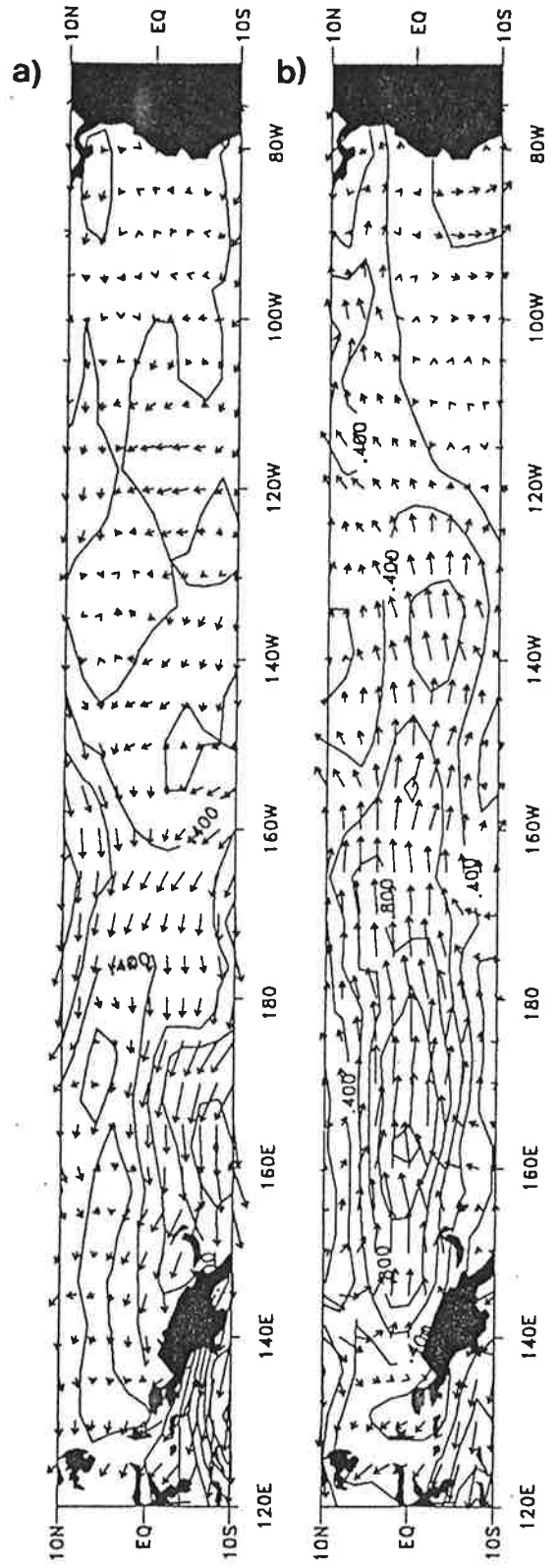

CONTOUR FROM 0.00000E+00 TO 4.0000 CONTOUR INTERVAL OF 0.20000 PT(3,3)= 0.98836

Figure 3: Associated regression patterns of the low-level wind field [m/s] on the coefficient time series of the Kelvin wave POP mode. a) Real part, b) imaginary part.

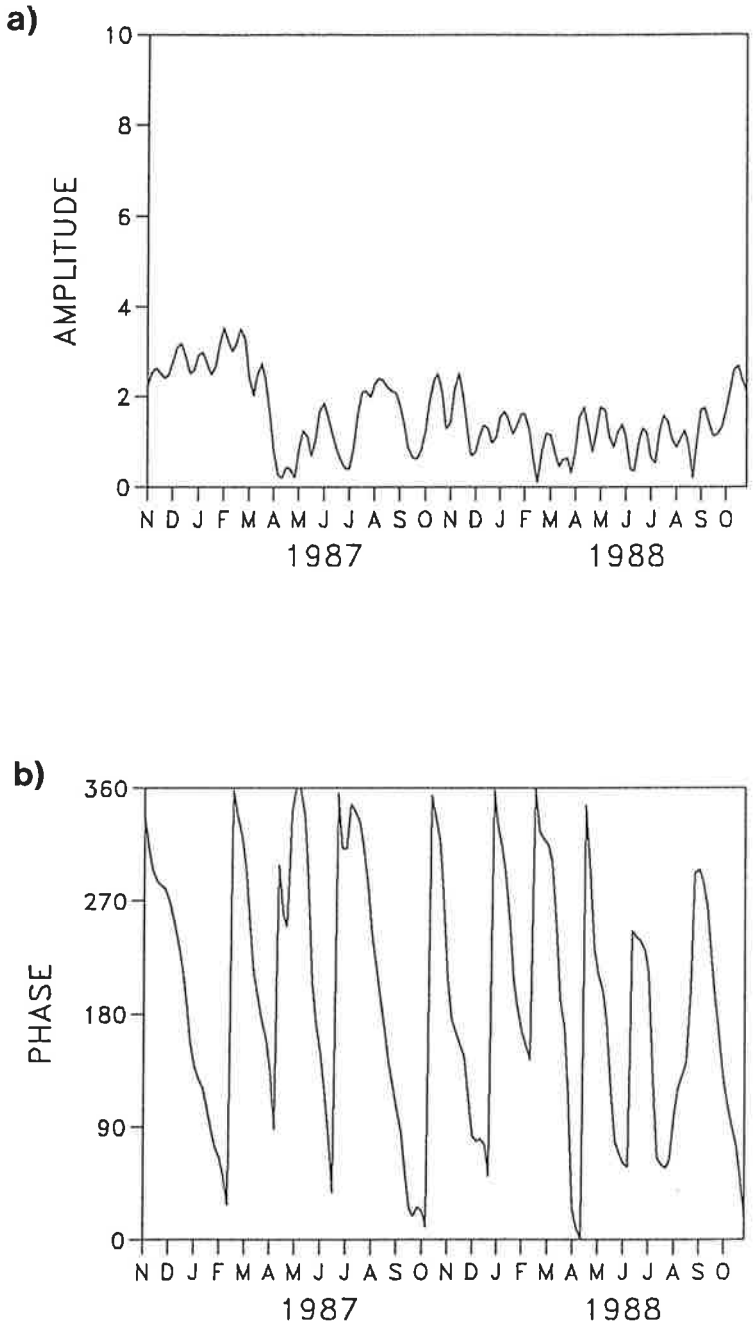

Figure 4: Amplitude (a) and phase (b) time series of the Kelvin wave POP mode.

in Table 2. Four variability modes were identified in the GEOSAT data, and these will now be described.

4.1 Kelvin wave mode

The highest frequency mode which was derived from the GEOSAT sea levels will be referred to as the "Kelvin wave" mode. Kelvin wave propagation was described in a case study by Miller et al. (1987), who analyzed the original GEOSAT altimeter data. The Kelvin wave mode explains 13 % of the variance in the band-pass filtered data and its POP period is 93 days, whereas the damping time amounts to 86 days. The POP period indicates that this POP mode is the oceanic counterpart of the atmospheric "30-60 day" oscillation (Madden and Julian (1972)), but it is still an open question why the period of the oceanic oscillation is shifted by about 30 days relative to the atmospheric oscillation (McPhaden and Taft (1988)). The two POP patterns (Fig. 2), consistent with equatorial Kelvin wave dynamics, exhibit equatorially trapped signals which propagate eastward along the equator with a speed of about 2.5 m/s. Thus, we conclude that this particular POP mode can be identified with the first baroclinic Kelvin wave mode which has a similar theoretical phase speed.

The associated regression pattern of the low-level wind field (Fig. 3) on the (complex) POP time series shows a strong westerly anomaly centered in the western equatorial Pacific near 160°E which lasts for a few weeks only (Fig. 3b). Such wind events in the western Pacific are related to the atmospheric 30-60 day oscillation and referred to as "wind bursts". The response of the equatorial Pacific to these wind bursts is described in several studies in which in-situ observations were analyzed (e. g. McPhaden and Taft (1988) and McPhaden et al. (1988)), and the results described in these studies are consistent with our findings. In particular, our results support the picture that on intraseasonal time scales sea level variability in the eastern Pacific is forced remotely by wind anomalies in the western Pacific. The amplitude time series of the Kelvin wave mode (Fig. 4a) indicates strongest activity during late 1986 and early 1987. This is consistent with the study of McPhaden et al. (1990), who found the strongest westerly wind burst activity during November and December 1986. The phase time series of the Kelvin wave mode

(Fig. 4b) is fairly regular, with about ten cycles during the analyzed period November 1986 to October 1988. The Kelvin wave mode is not simulated by the ocean model because monthly mean winds were used to force it so that wind bursts are not resolved.

3.2 Semi-annual cycle

The most energetic POP mode explaining 29 % of the variance in the band-pass filtered data has a rotation period of 187 days, i. e. about 6 months and a damping time of about 11 months. This mode represents the semi-annual cycle in equatorial Pacific sea level, as can be seen clearly from the POP phase time series (Fig. 7b). Spectra of zonal currents and sub-surface temperatures in the eastern Pacific which were derived from buoy measurements also indicate the existence of a strong semi-annual cycle (McPhaden and Taft (1988)). The POP patterns show the well known characteristics of equatorial waves (Figs. 5a and 5b). We therefore hypothesize that this mode represents the forced wave response of the equatorial Pacific to the semi-annual component of the surface wind stress. The imaginary part (Fig. 5a) is consistent with Rossby wave activity in the western Pacific and Kelvin wave activity in the eastern Pacific, with maximum anomalies off the equator in the west and at the equator in the east. Western boundary Rossby wave reflection is evident in the rotation from the imaginary to the real part (Fig. 5b), which shows a signal emanating from the western boundary and propagating eastward along the equator. Eastern boundary reflection of the incident Kelvin wave is also seen. The associated regression patterns of the low-level wind field (Fig. 6) show strong signals over the western and central equatorial Pacific only. This is the region where the semi-annual cycle in the wind stress has considerable amplitude (Goldenberg and O'Brien (1981), Horel (1982)).

A similar POP mode is found in the OGCM-run with observed wind stresses (Table 2). The rotation period is about 7 months, the damping time about 4 months, and the explained variance about 6 %. The POP patterns (not shown) show also the characteristic Rossby and Kelvin wave structure. Similar POP modes were also found in the two sensitivity experiments. In the first sensitivity experiment, in which the model was driven with random wind stress anomalies superimposed on a constant background wind stress without seasonal variation, a POP mode was found with a rotation period about 7 months. This POP mode

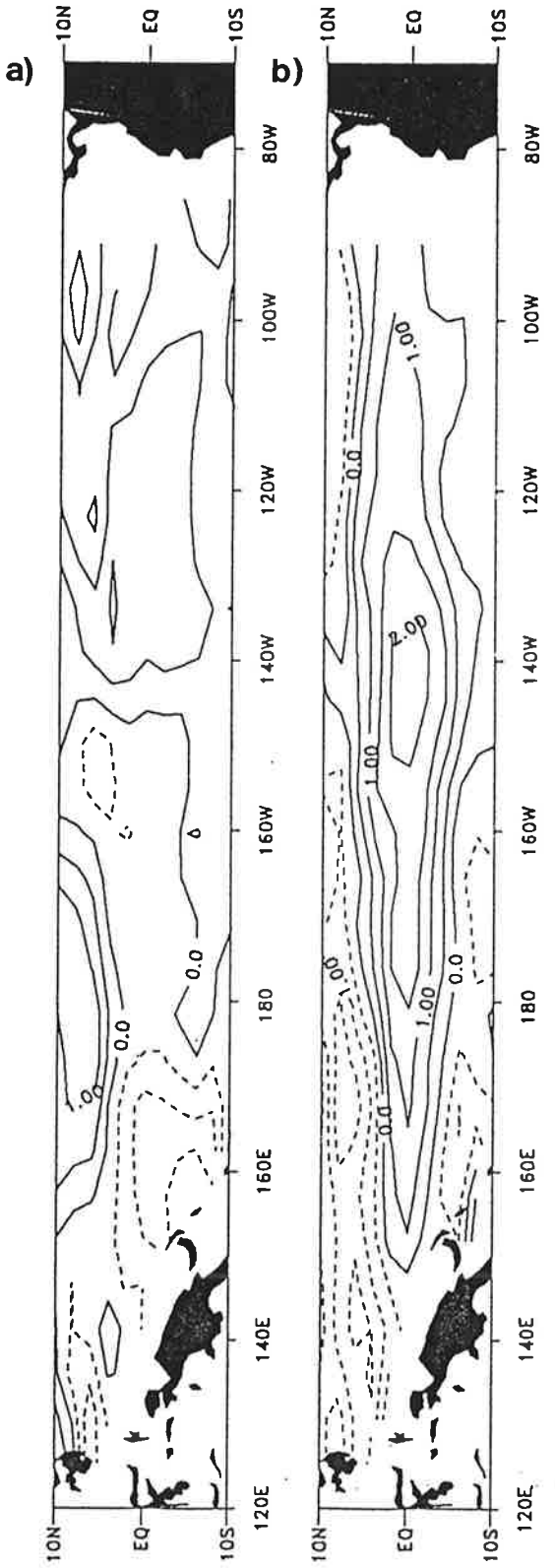

CONTOUR FROM -4.0000 TO 4.0000 CONTOUR INTERVAL OF 0.50000 PT(3,3)= 0.90000+100

Figure 5: Spatial patterns of the semi-annual cycle POP mode. a) Real part, b) imaginary part.

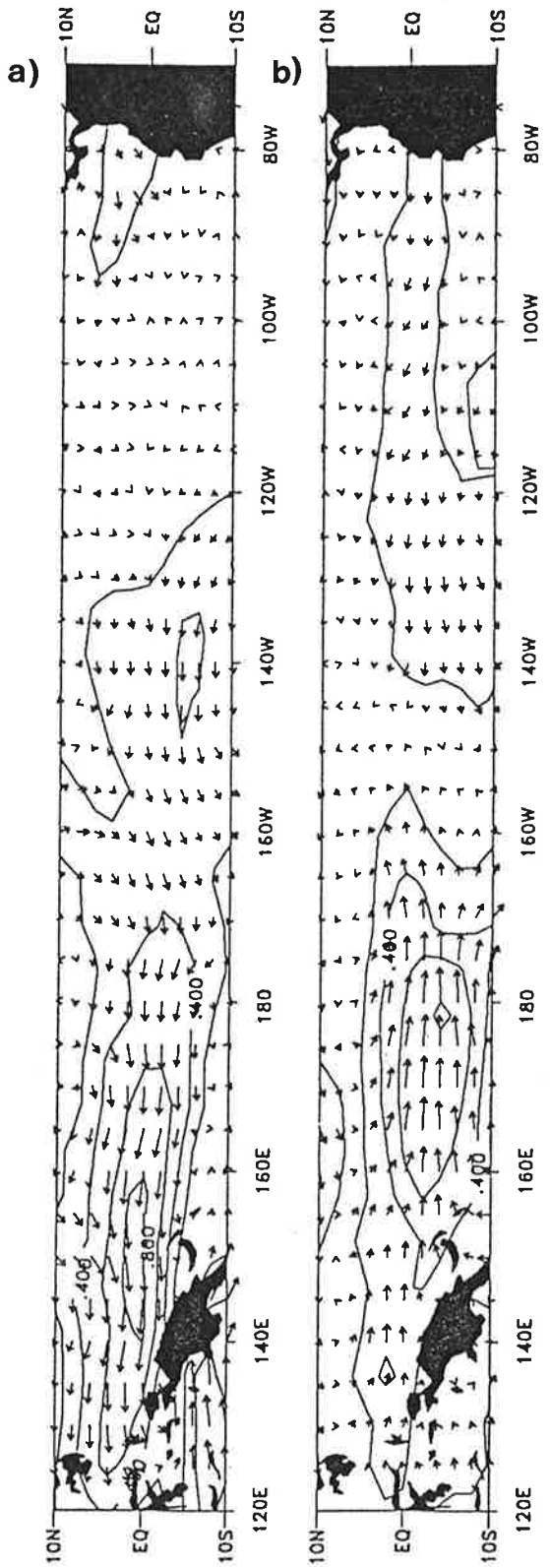

Figure 6: Associated regression patterns of the low-level wind field [m/s] on the coefficient time series of the semi-annual cycle POP mode. a) Real part, b) imaginary part.

reflects the gravest baroclinic basin mode of the equatorial Pacific. In the second sensitivity experiment, in which the OGCM was forced with the seasonal cycle of the wind stress only, a similar POP mode was found with a rotation period 6 months. This POP mode represents the forced ocean response to the semi-annual component of the wind stress. Thus, we conclude that sea level variability on time scales of about half a year is continuously excited by the semi-annual and the random components of the equatorial Pacific wind stress. Furthermore, since the gravest basin mode found in the first sensitivity experiment has a frequency close to that of the semi-annual cycle, some resonance between the gravest basin mode and the semi-annual cycle is to be expected.

Another mode was found in the ocean model data, explaining about 3% of the variance (not shown). The rotation period of this mode is about 11 months with a decay time of about 3 months. This mode was not found in the GEOSAT data and is associated with the propagation of the first meridionally antisymmetric Rossby wave (meridional mode j = 2). An investigation of the associated regression patterns of the zonal wind stress showed that this mode is forced by the meridionally antisymmetric component of zonal wind stress.

3.3 Annual cycle

We then low-pass filtered the data, extended the analysis to the region 20°N to 20°S, and considered the full time period, in order to derive the annual cycle and low-frequency variability. The annual cycle accounts for 17 % of the sea level variability in the low-pass filtered GEOSAT data. The POP period is estimated as 359 days and the damping time 594 days. The POP phase time series (Fig. 10b) indicates a fairly regular evolution of the annual cycle throughout the analyzed period. The annual cycle in sea level is mostly dominated by north-south variations, as can be inferred from the two POP patterns (Fig. 8). The changes are strongest in the vicinity of the two major convergence zones. In the northern hemisphere, changes are due to the seasonal migration of the Intertropical Covergence Zone (ITCZ), whereas annual variability in the southwestern Pacific is associated with movements of the South Pacific Convergence Zone (SPCZ) (Fg. 9).

Although the zonal wind stress is strongest during the extreme seasons (Fig.

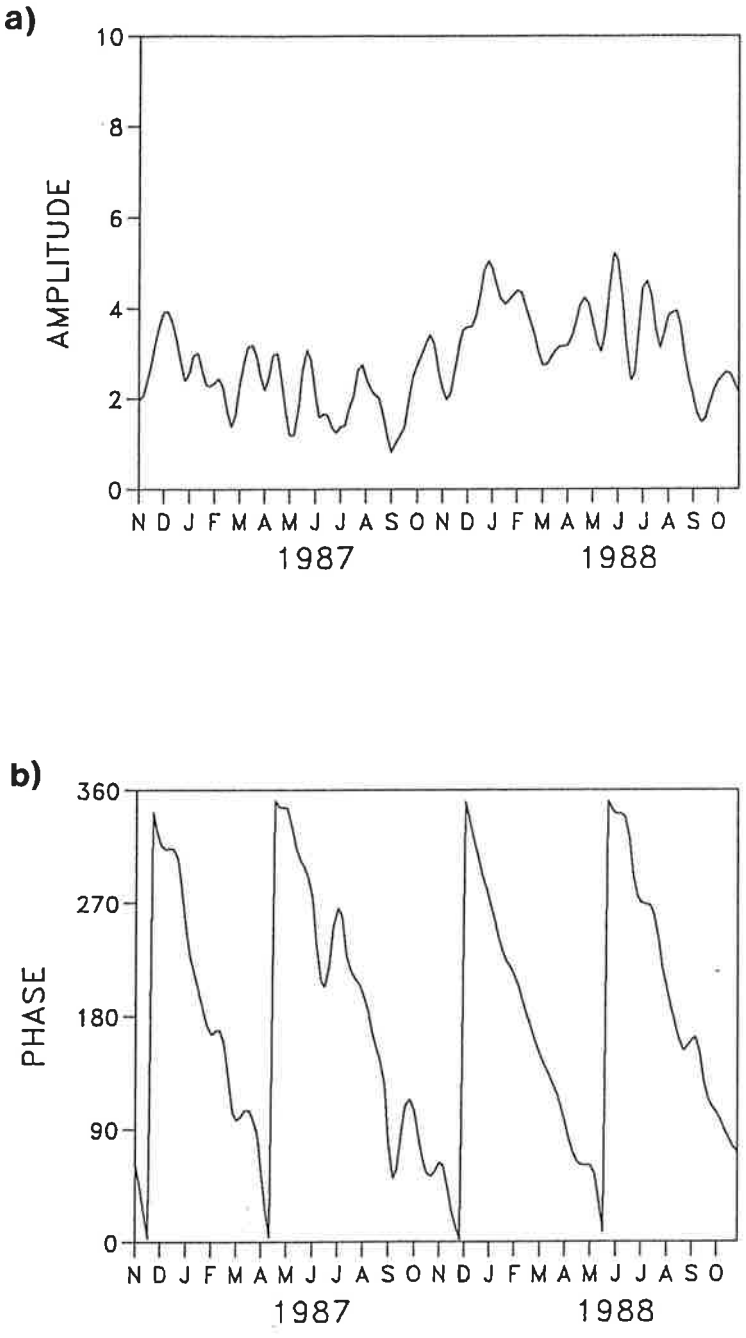

Figure 7: Amplitude (a) and phase (b) time series of the semi-annual cycle POP mode.

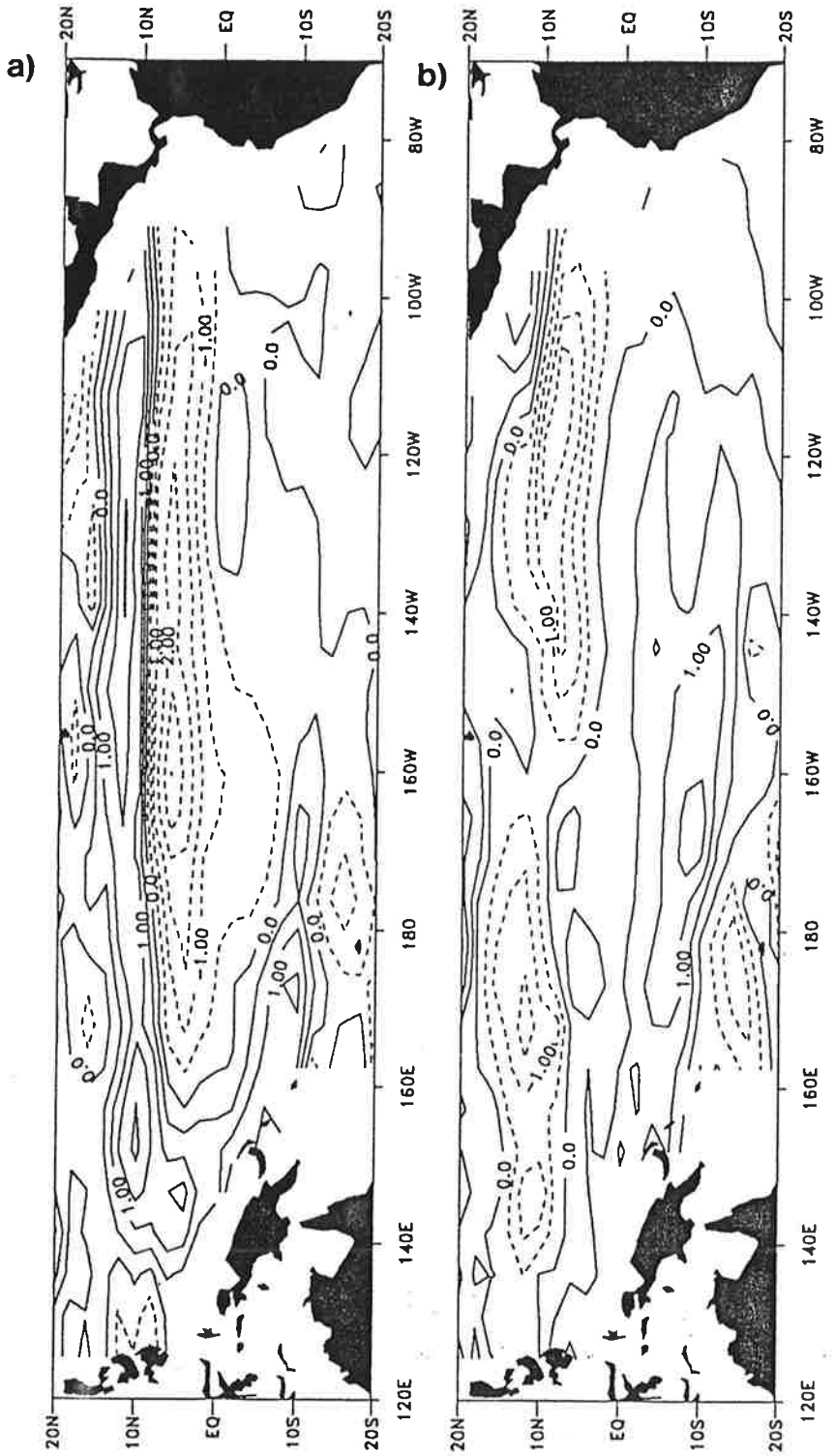

Figure 8: Spatial patterns of the annual cycle POP mode. a) Real part, b) imaginary part.

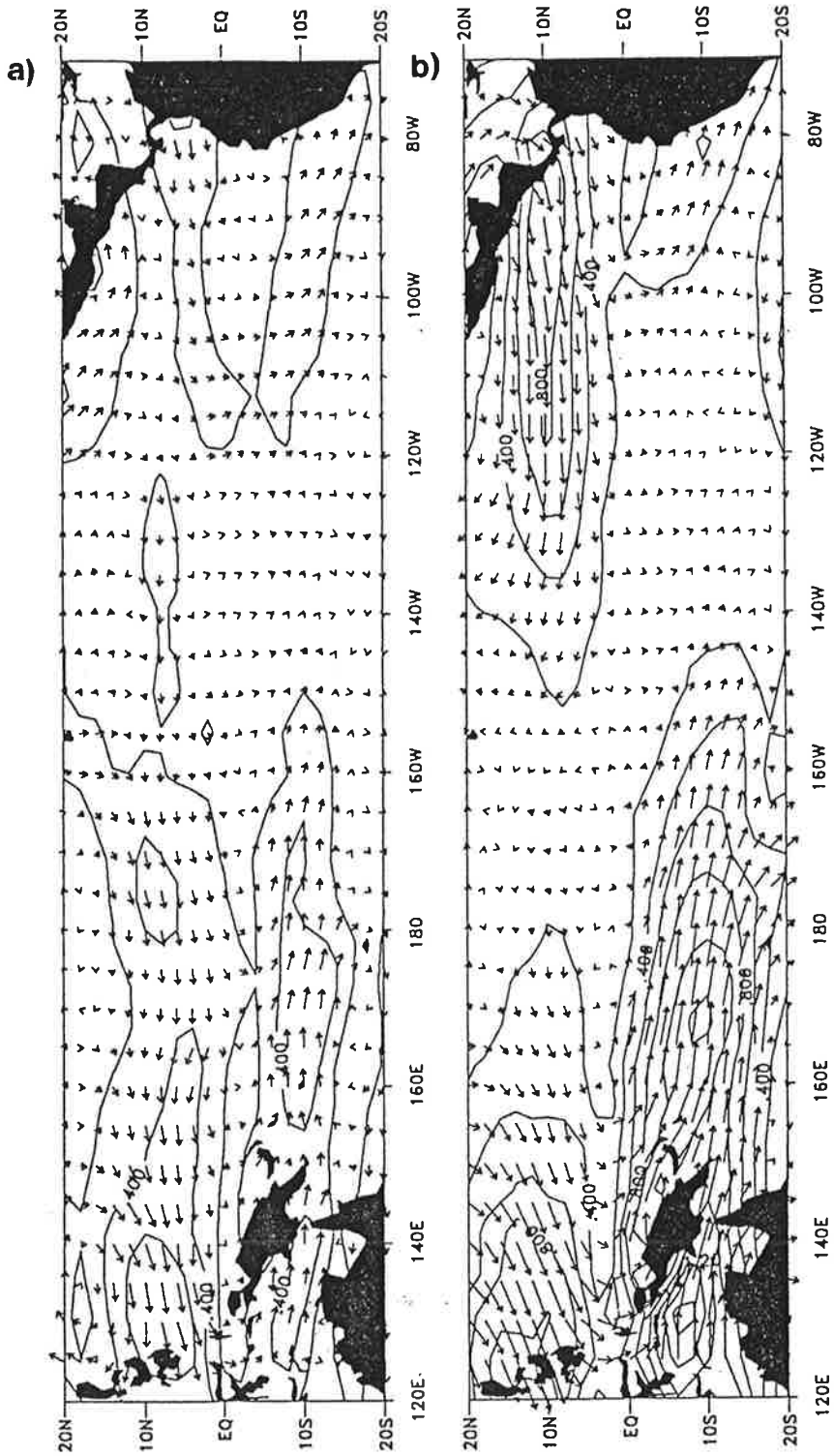

Figure 9: Associated regression patterns of the low-level wind field [m/s] on the coefficient time series of the annual cycle POP mode. a) Real part, b) imaginary part.

9b), it has its strongest impact on the sea level and the resulting geostrophic zonal surface currents during the transition seasons (Fig. 8a). As already discussed by Wyrtki (1974), the anomalies in the wind stress curl during the transition seasons are favourable for changing the mean ridge-trough structure in sea level, slowing down the currents in the northerm hemisphere in northern spring and amplifying them in northern fall (Fig. 8a). Let us consider the situation in spring, for instance. According to the real part of the annual cycle POP (Fig. 8a), both the Countercurrent Trough and the Equatorial Ridge are weakened, which leads to a weakening of the North Equatorial Countercurrent. Since the winds are light near the equator during this time of the year, the South Equatorial Current also attains a minimum in its speed. The same arguments hold for fall, but with reversed signs.

No evidence is found in the GEOSAT data for annual western boundary Rossby wave reflection, as hypothesized by White et al. (1990). Furthermore, the results of the POP analysis of the OGCM data does not show any evidence for annual Rossby wave reflection either. However, since western boundary reflection is important for the semi-annual cycle and the ENSO mode (described below), a proper modal description of the variability in the tropical Pacific requires a sophisticated statistical technique, such as the POP-technique.

In contrast to the GEOSAT data, the OGCM shows additionally that sea level anomalies propagate westward on both sides of the equator within the latitude band $8^{\circ}N$ - $8^{\circ}S$. This westward propagation arises from large-scale air-sea interactions. As described by Philander (1990) and Neelin (1991), spatial and temporal phase differences between SST and zonal wind stress are crucial for the westward phase propagation of the annual cycle near the equator, and physical processes within the surface mixed layer dominate wave processes. Although the corresponding spatial sea level structure is similar to equatorial wave structure, the zonal phase propagation should not be interpreted as Rossby wave propagation (Neelin (1991)).

3.4 ENSO mode

Finally, the interannual sea level variability is investigated. The dominant mode of interannual variability in the tropical Pacific is the El

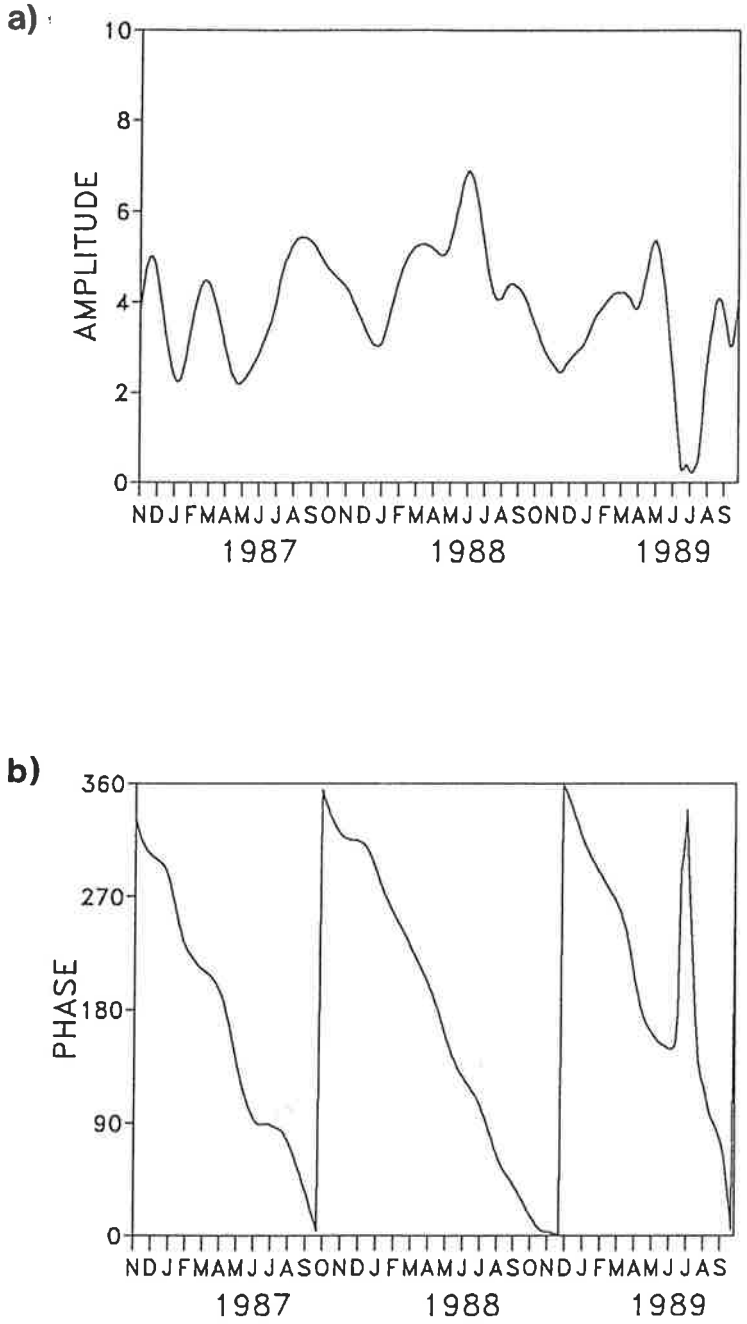

Figure 10: Amplitude (a) and phase (b) time series of the annual cycle POP mode.

Niño/Southern Oscillation (ENSO), which has a preferred recurrence time scale of about 4 years. However, recent observational and theoretical studies indicate that several time scales are involved in ENSO, predominantly a biennial time scale and one of the order of four years (e. g. Rasmusson et al. (1990), Barnett (1991), Münnich et al. (1991)). Although the GEOSAT data set is certainly not long enough to address adequately the ENSO-related interannual variability, the analyzed period is nevertheless sufficient for obtaining some insight into the nature of low-frequency variability, because it contains a major warm phase (1987) and a major cold phase (1988) of the ENSO cycle.

One interannual POP mode was found explaining about 27 % of the variance in the low-pass filtered data. This mode is clearly associated with the ENSO phenomenon and has a rotation period of 38 months and a damping time of 34 months. Similar low-frequency POP modes were derived from the island sea levels (Latif and Flügel (1991)) and the OGCM sea levels (Table 2). The OGCM POP mode has already been described by Latif and Villwock (1990). The real part (Fig. 11a) represents the conditions during the extreme phases of ENSO (El Niño and La Niña), when SST anomalies are fully developed in the eastern and central equatorial Pacific, and ocean and atmosphere interact strongly, while the imaginary part (Fig. 11b) shows conditions during the transition phases, when SST anomalies are near normal, and ocean-atmosphere coupling is of minor importance.

In the following, the evolution of anomalous conditions during the period November 1986 to August 1989 is reconstructed from the POP pair described in the last paragraph. Since sea level is a measure of upper ocean heat content, the evolution of the sea level field is equivalent to the horizontal redistribution of heat during this period. Conditions in late 1986 are given by the imaginary part (Fig. 11b), as can be inferred from the POP phase time series (Fig. 13b) which attains a phase angle of about 270° at this particular time. Positive heat content anomalies cover the entire equatorial strip between 5°N and 5°S and equatorial winds are near normal (Fig. 12b) during this time. This is consistent with a build-up of water above the thermocline prior to El Niño, as hypothesized by Wyrtki (1985). Conditions in the following May are to first order given by the real part (Fig. 11a), as indicated by the phase angle of about 180° (Fig. 13b). This period can be regarded as the height of the El Niño event, with negative heat content

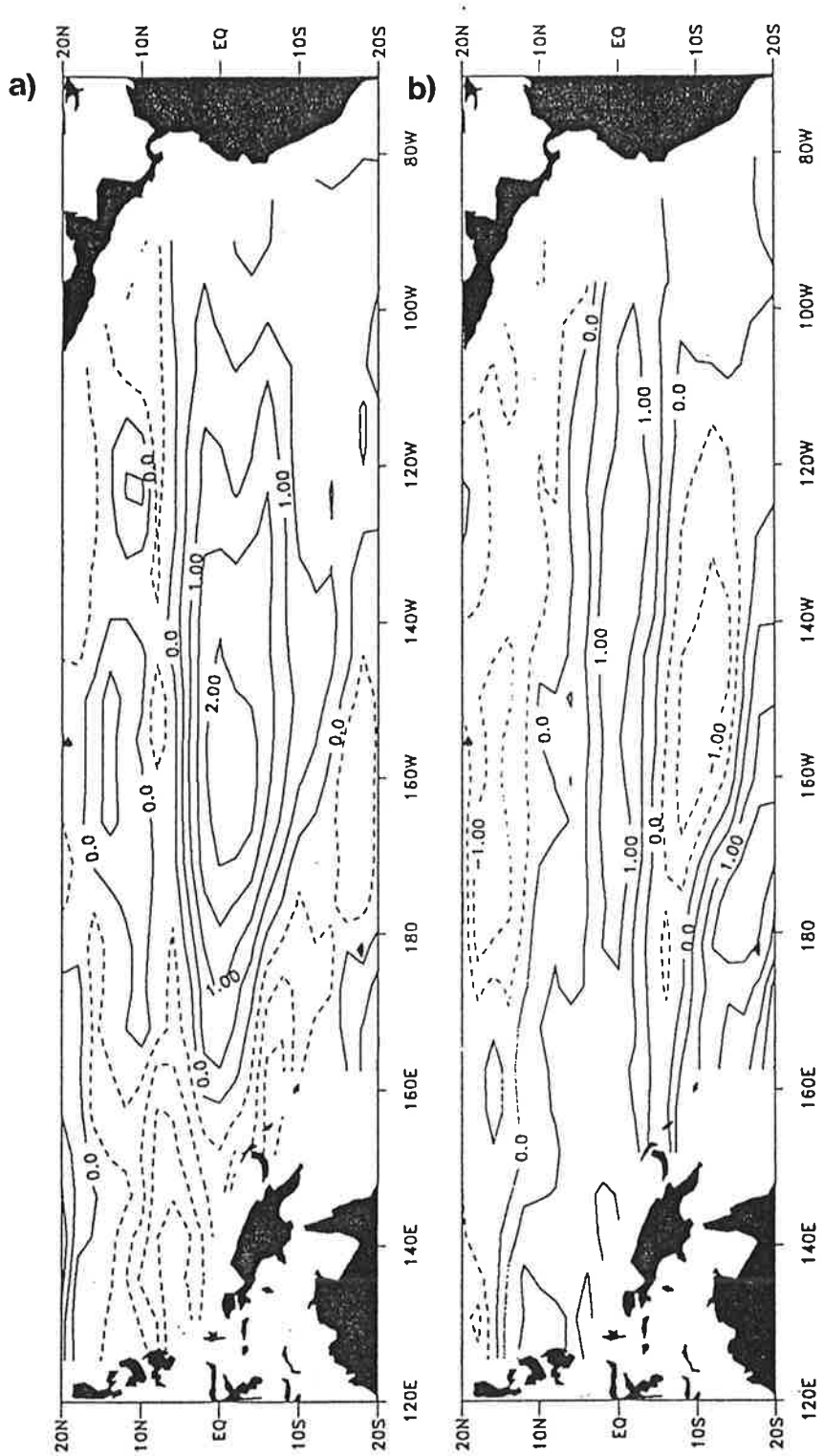

Figure 11: Spatial patterns of the ENSO POP mode. a) Real part, b) imaginary part.

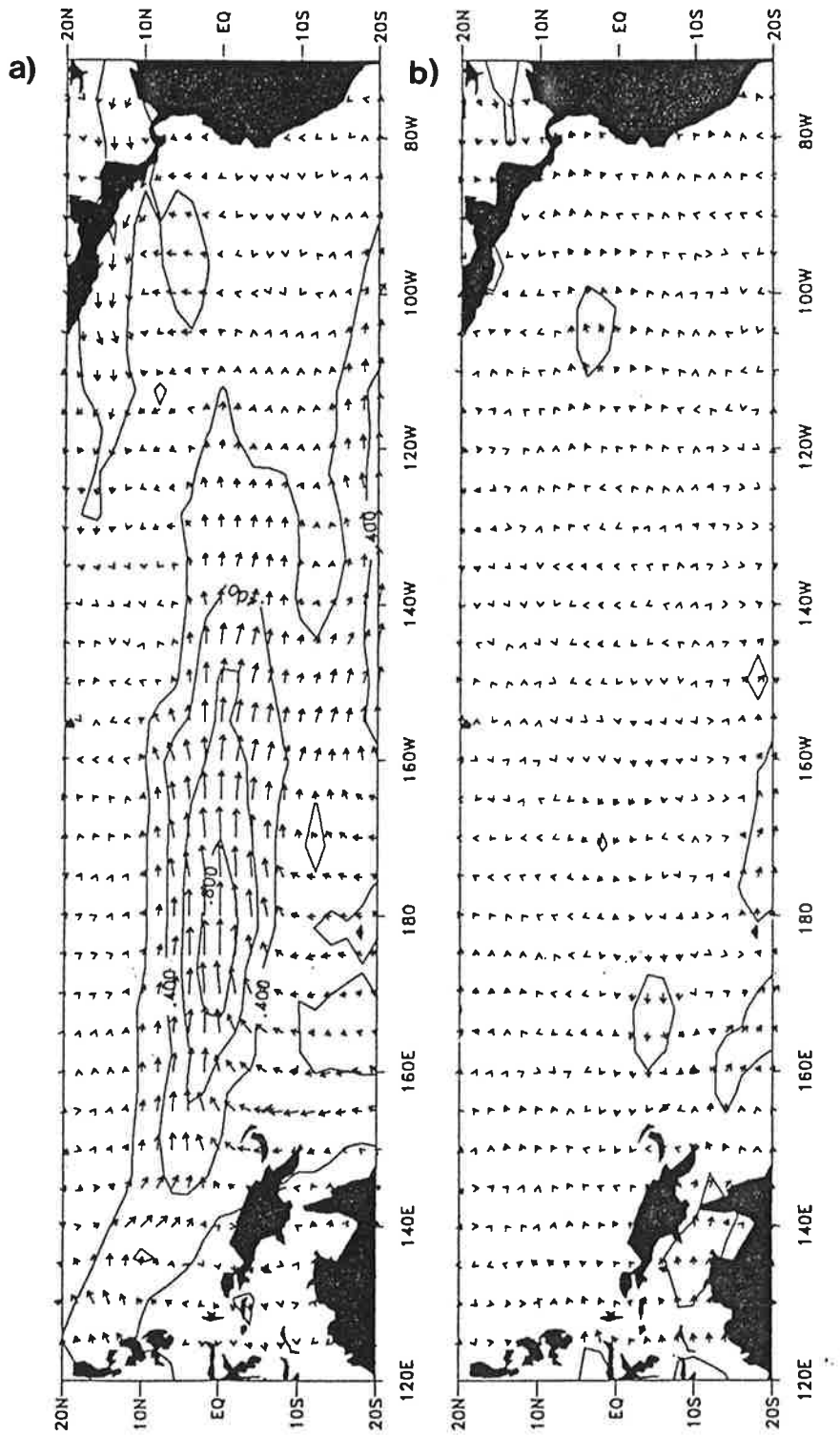

Figure 12: Associated regression patterns of the low-level wind field [m/s] on the coefficient time series of the ENSO POP mode. a) Real part, b) imaginary part.

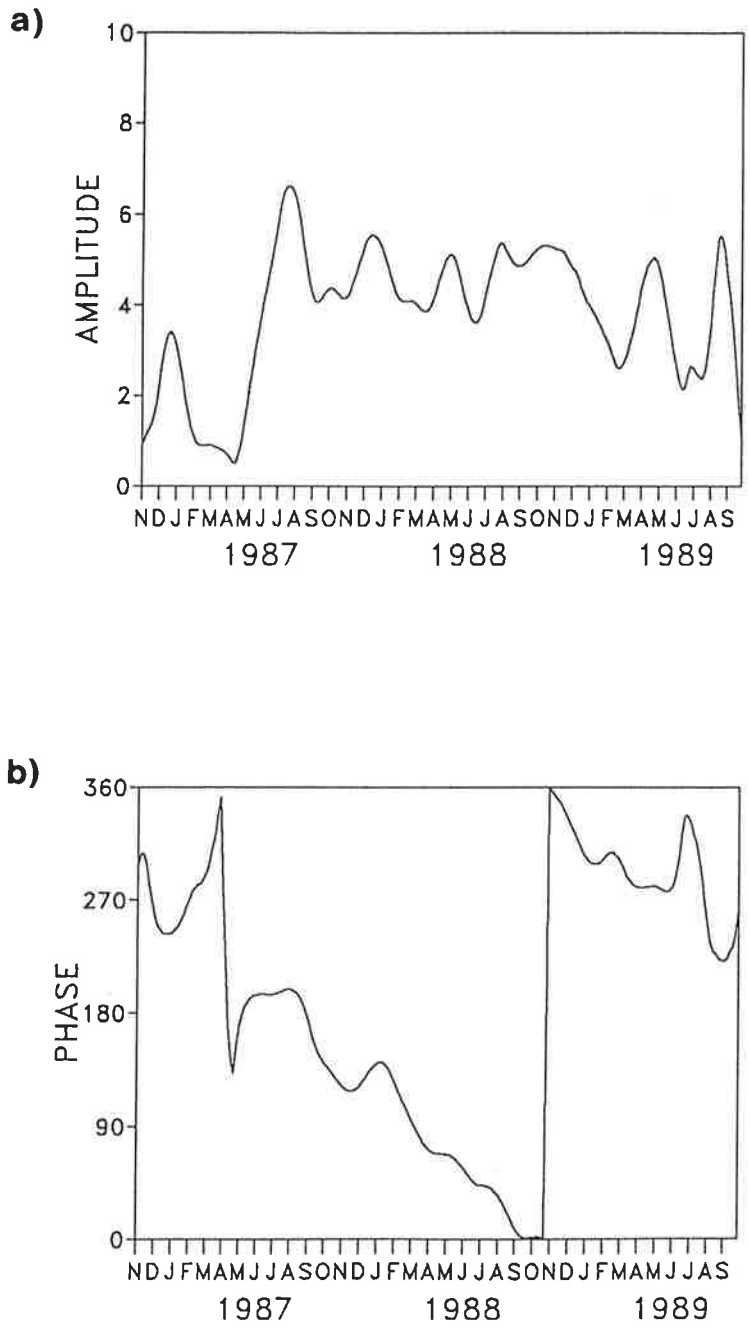

Figure 13: Amplitude (a) and phase (b) time series of the ENSO POP mode.

anomalies in the western and positive heat content anomalies in the eastern Pacific. The negative anomalies in the west are strongest off the equator, while those in the east are centered at the equator. The zonally asymmetric pattern is consistent with a reduced tilt of the sea surface across the Pacific and indicates a zonal redistribution of heat from west to east during the El Niño event. At this time, SST anomalies were well developed (see, for instance, the CAC Climate Diagnostics Bulletin) and westerly wind stress anomalies were observed over the western and central Pacific (see also Fig. 12a). The theoretical linear ocean response to such a westerly wind patch is very similar to that given by the imaginary part of the ENSO-POP. About 10 months later, conditions are given by the imaginary part (Fig. 11b, but with reversed signs), and the equatorial Pacific is drained of warm water, as indicated by the negative sea level anomalies which cover the equatorial Pacific. The low-level winds are near normal at this time (Fig. 12b). In late 1988 the cold phase of the ENSO cycle (La Niña) is fully developed with positive heat content anomalies in the west and negative heat content anomalies in the east (Fig. 11a, but with reversed signs).

The evolution of the anomalous conditions as derived from the GEOSAT data set is consistent with theoretical and observational studies. Sea level anomalies are found to be dominated by a propagating mode, whereas the low-level wind anomalies are governed by a standing component. These findings are consistent with the conceptual model of 'delayed action oscillation' (Schopf and Suarez (1988), Graham and White (1988), Philander (1990), Latif et al. (1993)). According to this picture, the propagation of equatorial waves and their reflection at the western boundary are essential for maintaining the oscillation. The ENSO variability derived from the GEOSAT data supports this view, but as described by Philander (1990), at low frequencies many wave modes are excited in the ocean so that the phase speeds would expected to be much slower than that of the gravest baroclinic mode. By following the anomalies between the two POP patterns, a phase speed of about 30 cm/s was estimated, which is in good agreement with the value given by Latif et al. (1993), who investigated 20 years of subsurface data. In summary, the interannual variability in sea level can be understood as the oceanic response to periodic low-frequency forcing by the atmosphere, as described analytically by Cane and Sarachik (1981).

4. Conclusions

Satellite derived (GEOSAT) sea level data were investigated for the period November 1986 to September 1989 in order to derive the dominant modes of climate variability in the tropical Pacific. Although the GEOSAT data set is rather short, it provides a proper modal decomposition of climate variability in the tropical Pacific. This was shown by comparing the variability modes derived from the GEOSAT data set with those derived from the output of an oceanic general cicrulation model (OGCM) which was forced by observed wind stresses for the period 1961 to 1988.

The sea level variability in the tropical Pacific can be mainly described in terms of four modes, a Kelvin wave mode, the semi-annual and annual cycles, and the El Niño/Southern Oscillation (ENSO) mode. The Kelvin wave and semi-annual mode can be viewed as the forced ocean responses to variations in equatorial zonal wind stress. Equatorial wave dynamics is crucial for these two modes. The annual cycle is dominated by Ekman dynamics, and equatorial wave dynamics appears to be unimportant. In particular, western boundary Rossby wave reflection was found neither in the GEOSAT nor in the model data. Furthermore, the qualitative seasonal changes in the geostrophic zonal surface currents, as derived from the seasonal sea level variations, are consistent with those described in earlier studies (e. g. Wyrtki (1974)). Changes in the wind stress curl during the transition seasons are the most likely reason for changes in the zonal surface currents, with the strongest currents occurring on the northern hemisphere in fall.

The El Niño/Southern Oscillation (ENSO) mode dominates the variability on interannual time scales. Although the GEOSAT record is very short, it was possible to extract from it a mode, which can be described as the oceanic response to periodic low-frequency atmospheric wind stress forcing (Cane and Sarachik (1981), Philander (1990)). A similar mode was found in other observational and model studies (e. g. Wyrtki (1985), Graham and White (1988), Latif and Flügel (1991), Blumenthal (1992), Latif et al. (1993)). Consistent with the 'delayed action oscillator' scenario, equatorial wave dynamics is important for the ENSO mode.

This study has shown that satellite-derived sea level data contain a large

amount of useful information, which can be used to continuously monitor the ocean. Furthermore, the satellite data are highly consistent with the output of an oceanic general circulation model, so that the benefit of the satellite measurements can be maximized by assimilating them into ocean circulation models. In the next stage, the analyzed ocean fields can be used as initial conditions for short-range climate predictions. This work is now underway and will be described in a forthcoming paper.

Acknowledgements

The authors would like to thank Prof. Dr. W. Alpers for his substantial contribution to this project and Dr. E. Maier-Reimer and Dr. H. von Storch for many fruitful discussions. We thank Dr. R. E. Cheney for providing the GEOSAT data and Dr. K. Arpe for providing the wind data. The help of Mr. Rainer Schnur in using the POP package is greatly acknowledged. Many thanks to Mrs. M. Grunert for preparing the diagrams. The ocean model runs were carried out at the "Deutsches Klimarechenzentrum". The work was supported by the European Community under grant EV5V-CT92-0121.

References

Barnett, T. P., 1991: The interaction of multiple time scales in the tropical climate system. J. Climate, 4, 269-285.

Barnett, T. P., M. Latif, E. Kirk, and E. Roeckner, 1991: On ENSO physics. J. Climate, 4, 487-515.

Blumenthal, M. B., 1991: Predictability of a coupled ocean-atmosphere model. J. Climate, 4, 766-784.

Bretherton, F. P., R. E. Davis, C. B. Fandry, 1976: A technique for objective analysis design of oceanographic experiments applied to Mode 73. Deep Sea Res., 23, 559-582.

Busalacchi, A. J., K. Takeuchi, and J. J. O'Brien, 1983: Interannual variability of the tropical Pacific. Hydrodynamics of the Equatorial Ocean. J. C. J. Nihoul Ed., Elsevier Oceanographic Ser., Vol. 40.

Cane, M. A. and E. S. Sarachik, 1981: The response of a linear baroclinic equatorial ocean to periodic forcing. J. Mar. Res., 39, 651-693.

Cheney, R. E. and L. Miller, 1990: Recovery of the sea level signal in the western tropical Pacific from Geosat altimetry. J. Geophys. Res., 95, 2977-2984.

Cheney, R. E., B. C. Douglas, and L. Miller, 1989: Evaluation of Geosat altimeter data with application to tropical Pacific sea level variability. J. Geophys. Res., 4737-4747.

Cheney, R. E., W. J. Emery, B. J. Haines, and F. Wentz, 1991: Recent improvements in Geosat altimeter data. Eos, 72, 51, 578-580.

Goldenberg, S. O. and J. J. O'Brien, 1981: Time and space variability of tropical Pacific wind stress. Mon. Wea. Rev., 109, 1190-1207.

Graham, N. E. and W. B. White, 1988: The El Nino cycle: A natural oscillator of the Pacific Ocean-Atmosphere system. Science, 240, 1293-1302.

Hasselmann, K., 1988: PIPs and POPs: The reduction of complex dynamical systems using Principal Interaction and Oscillation Patterns. J. Geophys. Res., 93, D9, 11015 - 11021.

Horel, J. D., 1982: On the annual cycle of the tropical Pacific atmosphere and ocean. Mon. Wea. Rev., 110, 1863-1878.

Journal of Geophysical Reseach, 1990: Special Volume on Geosat.

Latif, M., 1987: Tropical ocean circulation experiments. J. Phys. Oceanogr., 17, 246-263.

Latif M. and A. Villwock, 1990: Interannual variability in the tropical Pacific as simulated by coupled ocean-atmosphere models. J. Mar. Systems, 1, 51-60.

Latif, M. and M. Flügel, 1991: An investigation of short-range climate variability in the tropical Pacific. J. Geophys. Res., 96, 2661-2673.

Latif, M., A. Sterl, E. Maier-Reimer, and M. M. Junge 1992: Structure and predictability of the El Niño/Southern Oscillation phenomenon in a coupled ocean-atmosphere general circulation model. J. Climate, in press.

Legler, D. M. and J. J. O'Brien, 1984: Atlas of tropical Pacific wind stress climatology 1971-1980. Florida State University, Dept. of Meteorology, Tallahassee, U. S. A..

Madden, R. A. and P. R. Julian, 1972: Description of global-scale circulation cells in the tropics with a 40-50 day period. J. Atmos. Sci., 24, 1109-1123.

McPhaden, M. J. and B. A. Taft, 1988: Dynamics of seasonal and intraseasonal variability in the eastern equatorial Pacific. J. Phys. Oceanogr., 18, 1713-1732.

McPhaden, M. J., H. P. Freitag, S. P. Hayes, B. A. Taft, Z. Chen, and K. Wyrtki, 1988: The response of the equatorial Pacific Ocean to a westerly wind burst in May 1986. J. Geophys. Res., 93, 10589-10603.

McPhaden, M. J., S. P. Hayes, L. J. Magnum, J. M. Toole, 1990: Variability in the western Pacific Ocean during the 1986-87 El Niño/Southern Oscillation event. J. Phys. Oceanogr., 20, 190-208.

Miller, L. and R. E. Cheney, 1990: Large-scale meridional transport in the tropical Pacific Ocean during the 1986-1987 El Niño from Geosat. J. Geophys. Res., 95, 17905-17919.

Miller, L., R. E. Cheney, and B. C. Douglas, 1987: Geosat altimeter observations of Kelvin waves and the 1986-1987 El Niño. Science, 239, 52-54.

Münnich, M., M. A. Cane, and S. E. Zebiak, 1990: A study of self-excited oscillations of the tropical ocean-atmosphere system. Part II: Nonlinear cases. J. Atmos. Sci., 48, 1238-1248.

Neelin, J. D., 1991: The slow sea surface temperature mode and the fast-wave limit: analytic theory for tropical interannual oscillations and experiments in a hybrid coupled model. J. Atmos. Sci., 584-606.

Philander, S. G. H., 1990: A review of simulations of the Southern Oscillation. International TOGA Scientific Conference Proceedings (Honolulu, Hawaii, U. S. A., 16-20 July 1990). World Climate Research Programme, WCRP-43, WMO/TD-No. 379.

Picaut, J., A. J. Busalacchi, M. J. McPhaden, and B. Camusat, 1990: Validation of the geostrophic method for estimating zonal currents at the equator from Geosat altimeter data. J. Geophys. Res., 95, 3015-3024.

Reynolds, R. W., 1988: A real-time global sea surface temperature analysis. J. Climate, 1, 75-86.

Rasmusson, E. M., X. Wang, and C. F. Ropelewski, 1990: The biennial component of ENSO variability. J. Mar. Sys., 1, 71-96.

Schopf, P. S. and M. J. Suarez, 1988: Vacillations in a coupled ocean - atmosphere model. J. Atmos. Sci., 45, 549 - 566.

Storch, H. v., T. Bruns, I. Fischer-Bruns and K. Hasselmann, 1988: Principal Oscillation analysis of the 30 to 60 day oscillation in a GCM. J. Geophys. Res., 93, D9, 11022 - 11036.

Thai, C. K., 1988: Geosat crossover analysis in the tropical Pacific. 1. Constrained sinusoidal crossover adjustment. J. Geophys. Res., 93, 10621-10629.

Thai, C. K., W. B. White, and S. E. Pazan, 1989: Geosat crossover analysis in the tropical Pacific. 2. Verification analysis of altimetric sea level maps with expendable bathythermograph and Island sea level data. J. Geophys. Res., 94, 897-908.

White, W. B. and C. K. Tai, 1990: Reflection of interannual Rossby waves at the maritime western boundary of the tropical Pacific. J. Geophys. Res.

White, W. B., N. Graham, and C. K. Tai, 1990: Reflection of annual Rossby waves at the maritime western boundary of the tropical Pacific. J. Geophys. Res., 95, 3101-3116.

Wyrtki, K., 1974: Equatorial currents in the Pacific 1950 to 1970 and their relations to the trade winds. J. Phys. Oceanogr., 4, 372-380.

Wyrtki, K., 1985: Water displacements in the Pacific and the genesis of El Niño cycles. J. Geophys. Res., 90, 7129-7132.

Wyrtki, K., K. Constantine, B. J. Kilonsky, G. Mitchum, B. Miyamoto, T. Murphy, S. Nakahara, and P. Caldwell, 1988: The Pacific island sea level network. JIMAR Contr. 88-0137, Data Rep. 002, University of Hawaii, Honolulu.